BRL-TR-3318

2

TECHNICAL REPORT BRL-TR-3318

BRL

THE EFFECT OF FINITE CONDUCTIVITY ON MHD INSTABILITIES IN AXISYMMETRIC SHAPED CHARGE JETS

DAVID L. LITTLEFIELD

MARCH 1992

U.S. ARMY LABORATORY COMMAND

BALLISTIC RESEARCH LABORATORY
ABERDEEN PROVING GROUND, MARYLAND

NOTICES

Destroy this report when it is no longer needed. DO NOT return it to the originator.

Additional copies of this report may be obtained from the National Technical Information Service, U.S. Department of Commerce, 5285 Port Royal Road, Springfield, VA 22161.

The findings of this report are not to be construed as an official Department of the Army position, unless so designated by other authorized documents.

The use of trade names or manufacturers' names in this report does not constitute indorsement of any commercial product.

REPORT DOCUMENTATION PAGE

Form Approved
OMB No. 0704-0188

1. AGENCY USE ONLY (Leave blank)	2. REPORT DATE	3. REPORT TYPE AND DATES COVERED
	March 1992	Final, Oct 89 - Sep 90

4. TITLE AND SUBTITLE

The Effect of Finite Conductivity on MHD Instabilities in Axisymmetric Shaped Charge Jets

5. FUNDING NUMBERS

PR: 1L161102AH43

6. AUTHOR(S)

David L. Littlefield

7. PERFORMING ORGANIZATION NAME(S) AND ADDRESS(ES)

8. PERFORMING ORGANIZATION REPORT NUMBER

9. SPONSORING / MONITORING AGENCY NAME(S) AND ADDRESS(ES)

U.S. Army Ballistic Research Laboratory
ATTN: SLCBR-DD-T
Aberdeen Proving Ground, MD 21005-5066

10. SPONSORING / MONITORING AGENCY REPORT NUMBER

BRL-TR-3318

11. SUPPLEMENTARY NOTES

12a. DISTRIBUTION / AVAILABILITY STATEMENT

Approved for public release; distribution is unlimited.

12b. DISTRIBUTION CODE

13. ABSTRACT (Maximum 200 words)

In an earlier report by Powell and Littlefield, the effect of azimuthal magnetic fields on the stability of an axisymmetric shaped charge jet was investigated, assuming the magnetic Reynolds number was very large. Typical magnetic Reynolds numbers for shaped charge jets, however, are approximately 10, which is not large enough to justify the assumption. The present study relaxes this assumption to determine the effects of finite conductivity on the stability of the jet. An axial electric current is introduced in the jet at time $t = 0$ and permitted to diffuse over time. Linear perturbation theory is employed to determine the time evolution of small disturbances to the idealized motion of the jet. Solutions to the first-order equations indicate that disturbances in the magnetic field and pressure distributions vary significantly, depending on the magnetic Reynolds number. The growth rate in perturbations to the boundary, however, indicates that jets of finite conductivity are only slightly more stable than equivalent jets of infinite conductivity. The behavior of these instabilities is discussed in terms of the applicable physical mechanisms.

14. SUBJECT TERMS

electromagnetic disruption, shaped charge jets, jet stability, MHD stability, magnetic fields

15. NUMBER OF PAGES

29

16. PRICE CODE

17. SECURITY CLASSIFICATION OF REPORT	18. SECURITY CLASSIFICATION OF THIS PAGE	19. SECURITY CLASSIFICATION OF ABSTRACT	20. LIMITATION OF ABSTRACT
UNCLASSIFIED	UNCLASSIFIED	UNCLASSIFIED	UL

INTENTIONALLY LEFT BLANK.

TABLE OF CONTENTS

INTENTIONALLY LEFT BLANK.

LIST OF FIGURES

INTENTIONALLY LEFT BLANK.

Acknowledgment

The author is grateful to Dr. John D. Powell for many fruitful discussions and suggestions during the course of this research. This work was done while the author held a National Research Council-U. S. Army Ballistic Research Laboratory Research Associateship.

INTENTIONALLY LEFT BLANK.

1. INTRODUCTION

The instability and eventual breakup of shaped-charge jets have been previously observed in many experimental studies. These jets are commonly formed from the collapse of thin metallic conical liners, when exposed to the detonation of a high explosive. After formation, shaped-charge jets stretch with a reasonably uniform velocity gradient, when measured along their length. Apparently, this stretching motion is unstable, because after a specified time period (the *breakup time*) the jet will neck down in places along its surface and break into many fragments.

Interest in the breakup phenomenon observed in shaped-charge jets has prompted a number of theoretical investigations into the stability of elongating jets. Recent two-dimensional calculations by Curtis (1987), Pack (1988), and Romero (1989), in which the jet was assumed to be perfectly plastic and obey the Von-Mises yield criterion, have been successful in reproducing some of the behavior observed in experiments. These studies also accounted for inertial effects, since they are significant for shaped-charged jets, where strain rates as high as 10^5 sec^{-1} are commonly observed. The results indicated that uniformly elongating plastic jets are almost always unstable when a perturbation is introduced. Romero concluded that the most unstable disturbances for jets with large strain rates have initial wavelengths that are on the order of the jet diameter. This prediction is consistent with the experimental evidence for shaped-charge jets, where roughly equal-sized fragments have been observed after the jet breakup has initiated. A later study by Littlefield and Powell (1990) which also included electromagnetic effects, discussed in some detail the physical mechanisms responsible for this breakup.

Recent attention has focused on the development of methods for enhancement of the instabilities in shaped-charge jets, in order to reduce the breakup time. One proposed method involves the introduction of an axial electric current in the jet. By passing an axial current through the jet, it is hoped that instabilities similar to those found in plasma columns (Kruskal and Schwartzschild 1954; Tayler 1956) might be activated. Recent experiments have demonstrated that electrical currents may have an effect on the breakup time of jets Moreover, the study by Littlefield and Powell, in which a linear perturbation analysis was employed to examine the stability of infinitely conducting jets, indicated that electrical currents may shorten the breakup time of the jet. Further study is needed, however, before any definite conclusions can be drawn. The applicability of the analysis by Littlefield and Powell, for example, is limited due to the assumption of infinite conductivity. A typical copper shaped-charge jet (Powell and Littlefield 1990) has a conductivity of about 10^7 $(ohm\text{-}m)^{-1}$. The magnetic Reynolds number associated with the jet, therefore, is about ten, which

is not large enough to justify the infinite conductivity assumption.

The present analysis extends the previous work by Littlefield and Powell to include jets of finite conductivity. As in previous analyses, the jet is assumed to be infinitely long, uniformly elongating in the axial direction, and perfectly plastic. Heat conduction, dissipation, and Joule heating effects are also neglected, which permits the omission of the conservation of thermal energy and simplifies the analysis. In practice, this assumption restricts the electrical current to levels that are not large enough to cause large scale changes in the thermal energy. Two different base solutions for the velocity, pressure and magnetic field distributions are determined for the jet, as well as the surrounding vacuum, under axisymmetric conditions. In the first solution, an axial electric current, assumed to be initially on the surface, is permitted to diffuse into the jet interior over time. The second solution, on the other hand, assumes an initial body current, so that the axial current density is constant throughout the cross section. While the first solution is characteristic of the actual current distribution in jets, the second solution provides useful insights about the stability and facilitates the discussion. Small axisymmetric disturbances of these base solutions are then considered, and the equations governing their time evolution are derived using linear perturbation theory. Solutions to these equations are used to evaluate the stability of the jet.

The arrangement of this paper is as follows. In Sec. 2, the physical model is described and the governing equations in the jet, as well as the vacuum, are presented. Base solutions to these equations are given in Sec. 3 for the different initial current distributions. The first-order equations corresponding to these base solutions are derived in Sec. 4 using linear perturbation theory. In Sec. 5, these equations are solved and the stability characteristics of the jet are discussed. Finally, Sec. 6, contains some general conclusions and observations.

2. MATHEMATICAL MODEL

Consider an axisymmetric shaped-charge jet as depicted in Fig. 1. The jet is assumed to be uniformly elongating and perfectly plastic. A constant axial electric current I is passed through the jet initially and permitted to diffuse with time. The radius at any point along the jet boundary is denoted by $r_b(z,t)$, and the outward unit normal vector at this point by $\mathbf{n}$. The governing equations of motion in the jet, which may be found elsewhere (Powell and Littlefield 1990; Littlefield and Powell 1990) are repeated here for convenience. Let the velocity be given by $\mathbf{V}$, the pressure by p, the deviatoric stress tensor by $\Im$, the current density by $\mathbf{J}$, the electric field by $\mathbf{E}$, the magnetic-induction field by $\mathbf{B}$, the density by ρ, the conductivity by σ, and the magnetic permeability by μ_0. Then the governing equations are given by

$$\nabla \cdot \mathbf{V} = 0, \tag{1}$$

$$\rho\left(\frac{\partial \mathbf{V}}{\partial t} + \mathbf{V}\cdot\nabla\mathbf{V}\right) = -\nabla p + \nabla\cdot\Im + \mathbf{J}\times\mathbf{B}, \tag{2}$$

$$\mathbf{E} + \mathbf{V}\times\mathbf{B} = \mathbf{J}/\sigma, \tag{3}$$

$$\nabla\cdot\mathbf{B} = 0, \tag{4}$$

$$\nabla \times \mathbf{B} = \mu_0\mathbf{J}, \tag{5}$$

and

$$\nabla \times \mathbf{E} = -\frac{\partial \mathbf{B}}{\partial t}. \tag{6}$$

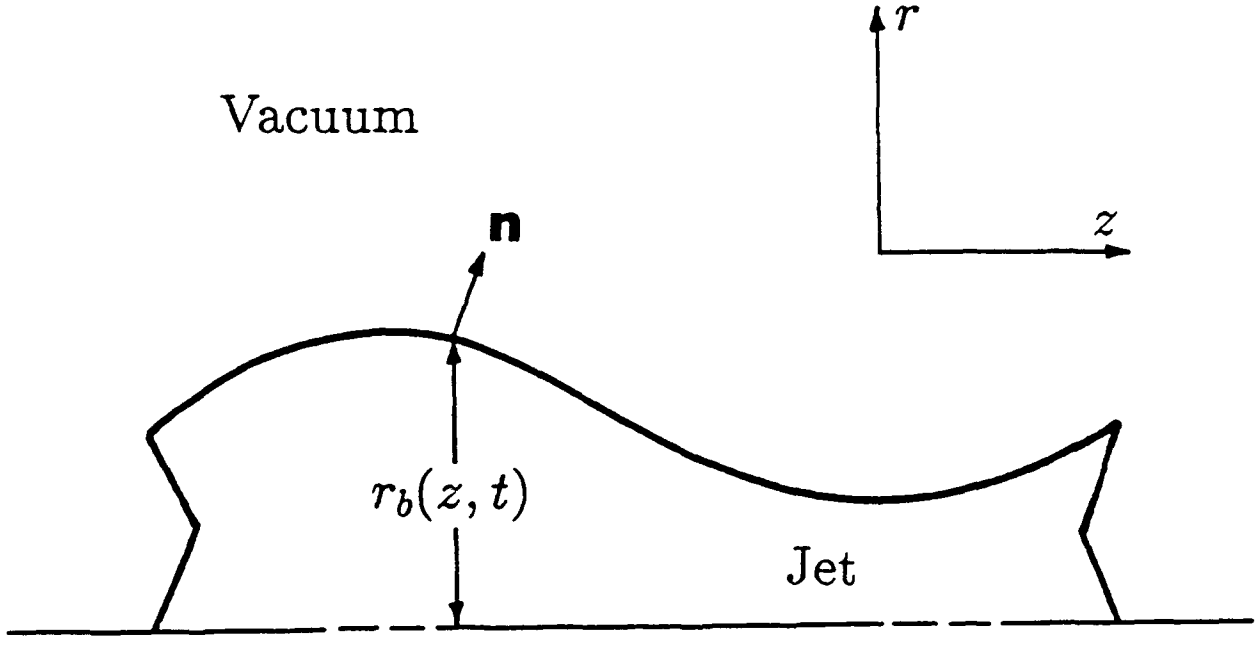

Figure 1. Model for jet stability calculations.

Equations (1) and (2) are the incompressible continuity and momentum equations, respectively; Eq. (3) is Ohm's Law, and Eqs. (4) - (6) are Maxwell's equations.

The present analysis assumes the idealized motion of the jet, as well as disturbances to this motion, are axisymmetric. Furthermore, J_θ and E_θ are assumed zero.* Consequently, the component forms of the governing equations may be simplified. The continuity equation, for example, reduces to

$$\frac{1}{r}\frac{\partial}{\partial r}(rv_r) + \frac{\partial v_z}{\partial z} = 0, \tag{7}$$

where v_r and v_z are the radial and axial components of the velocity, respectively. Ampère's law, given in Eq. (5), yields the two scalar relations

$$\frac{\partial B}{\partial z} = -\mu_0 J_r \tag{8}$$

and

$$\frac{1}{r}\frac{\partial}{\partial r}(rB) = \mu_0 J_z, \tag{9}$$

where J_r and J_z are the radial and axial components of the current density, respectively, and B is the azimuthal component of the magnetic field. With use of Eqs. (8) and (9), the component forms of the momentum equation become

$$\rho\left(\frac{\partial v_r}{\partial t} + v_r\frac{\partial v_r}{\partial r} + v_z\frac{\partial v_r}{\partial z}\right) = -\frac{\partial p}{\partial r} + \frac{\partial s_{rr}}{\partial r} + \frac{s_{rr} - s_{\theta\theta}}{r} + \frac{\partial s_{rz}}{\partial z} - \frac{1}{r}\frac{B}{\mu_0}\frac{\partial}{\partial r}(rB) \tag{10}$$

and

$$\rho\left(\frac{\partial v_z}{\partial t} + v_r\frac{\partial v_z}{\partial r} + v_z\frac{\partial v_z}{\partial z}\right) = -\frac{\partial p}{\partial z} + \frac{\partial s_{rz}}{\partial r} + \frac{s_{rz}}{r} + \frac{\partial s_{rz}}{\partial z} - \frac{B}{\mu_0}\frac{\partial B}{\partial z}, \tag{11}$$

where $s_{\alpha\beta}$ denotes the corresponding component of $\mathfrak{S}$. Ohm's Law yields the two component equations

$$\sigma(E_r - v_z B) = J_r \tag{12}$$

and

*The governing equations allow for nonzero J_θ and E_θ, but it may be shown these quantities tend to zero as time progresses anyway. Consequently, the contribution of nonzero J_θ and E_θ to the stability characteristics of the jet is believed to be small.

$$\sigma(E_z + v_r B) = J_z, \tag{13}$$

where E_r and E_z are the radial and axial components of the electric field, respectively. Eq. (4) yields information uncoupled from the present analysis, but (6) yields the single equation

$$\frac{\partial E_r}{\partial z} - \frac{\partial E_z}{\partial r} = -\frac{\partial B}{\partial z}. \tag{14}$$

The scalar forms of Eqs. (1) - (6), given in Eqs. (7) - (14), still have more unknowns than equations. A constitutive relationship must also be specified, relating the deviatoric stress to material properties and other variables in the jet. In the present analysis, the jet is assumed perfectly plastic. This requires the deviatoric stress to be proportional to the strain rate, which under axisymmetric conditions yields

$$s_{rr} = 2\lambda \frac{\partial v_r}{\partial r}, \tag{15}$$

$$s_{\theta\theta} = 2\lambda \frac{v_r}{r}, \tag{16}$$

$$s_{zz} = 2\lambda \frac{\partial v_z}{\partial z} \tag{17}$$

and

$$s_{rz} = \lambda \left(\frac{\partial v_r}{\partial z} + \frac{\partial v_z}{\partial r} \right), \tag{18}$$

where the coefficient of proportionality λ is formulated to satisfy the Von Mises yield criterion, given by

$$(s_{rr} - s_{\theta\theta})^2 + (s_{\theta\theta} - s_{zz})^2 + (s_{zz} - s_{rr})^2 + 6s_{rz}^2 = 2Y^2, \tag{19}$$

and Y is the constant yield strength. Solving for λ from Eq. (19) with use of Eqs. (15) - (18) gives

$$\lambda = \frac{Y}{\sqrt{3}} \left[2\left(\frac{\partial v_r}{\partial r}\right)^2 + 2\left(\frac{v_r}{r}\right)^2 + 2\left(\frac{\partial v_z}{\partial z}\right)^2 + \left(\frac{\partial v_r}{\partial z} + \frac{\partial v_z}{\partial r}\right)^2 \right]^{-\frac{1}{2}}. \tag{20}$$

Application of these constitutive relations to the momentum equations given in Eqs. (10) and (11) yields

$$\rho\left(\frac{\partial v_r}{\partial t}+v_r\frac{\partial v_r}{\partial r}+v_z\frac{\partial v_r}{\partial z}\right)=-\frac{\partial p}{\partial r}+\lambda\left(\frac{\partial^2 v_r}{\partial r^2}+\frac{1}{r}\frac{\partial v_r}{\partial r}-\frac{v_r}{r^2}+\frac{\partial^2 v_r}{\partial z^2}\right)$$

$$+2\frac{\partial\lambda}{\partial r}\frac{\partial v_r}{\partial r}+\frac{\partial\lambda}{\partial z}\left(\frac{\partial v_r}{\partial z}+\frac{\partial v_z}{\partial r}\right)-\frac{1}{r}\frac{B}{\mu_0}\frac{\partial}{\partial r}(rB), \tag{21}$$

and

$$\rho\left(\frac{\partial v_z}{\partial t}+v_r\frac{\partial v_z}{\partial r}+v_z\frac{\partial v_z}{\partial z}\right)=-\frac{\partial p}{\partial z}+\lambda\left(\frac{\partial^2 v_z}{\partial r^2}+\frac{1}{r}\frac{\partial v_z}{\partial r}+\frac{\partial^2 v_z}{\partial z^2}\right)$$

$$+2\frac{\partial\lambda}{\partial z}\frac{\partial v_z}{\partial z}+\frac{\partial\lambda}{\partial r}\left(\frac{\partial v_r}{\partial z}+\frac{\partial v_z}{\partial r}\right)-\frac{B}{\mu_0}\frac{\partial B}{\partial z}, \tag{22}$$

with λ given by Eq. (20). It is also convenient to combine Eqs.(8) - (9) and (12) - (14) into a single equation for B, which yields

$$\frac{\partial B}{\partial t}+v_r\frac{\partial B}{\partial r}-\frac{v_r B}{r}+v_z\frac{\partial B}{\partial z}=\frac{1}{\sigma\mu_0}\left(\frac{\partial^2 B}{\partial r^2}+\frac{1}{r}\frac{\partial B}{\partial r}-\frac{B}{r^2}+\frac{\partial^2 B}{\partial z^2}\right). \tag{23}$$

Eqs. (7) and (20) - (23) represent five equations for the five scalar unknowns (v_r, v_z, p, λ, and B) which govern the motion in the interior of the jet.

The relevant conservation equations also must be satisfied in the vacuum surrounding the jet. In the vacuum, Eq. (1) is meaningless and Eq. (2) is identically satisfied since ρ, p, $\mathfrak{F}$, and $\mathbf{J}$ are zero. Eqs. (3) - (6) may be simplified by setting $\mathbf{J}=\sigma=0$ and requiring axisymmetry. The resulting equation for B^v, the θ component of $\mathbf{B}$ in the vacuum, is given by

$$\frac{\partial^2 B^v}{\partial r^2}+\frac{1}{r}\frac{\partial B^v}{\partial r}-\frac{B^v}{r^2}+\frac{\partial^2 B^v}{\partial z^2}=0. \tag{24}$$

The remaining variables in the vacuum are either zero or may be determined by back substitution.

The application of these equations implies that certain conditions must be satisfied at the interface between the vacuum and the jet. In particular, mass and momentum must be

conserved and Maxwell's equations must be satisfied across the interface. These conditions may be derived systematically (Kruskal and Schwartzschild 1954) by integrating the relevant equations across the boundary, of presumed thickness δ, in a direction normal to the boundary, then taking the limit as $\delta \rightarrow 0$. Let dl be an element of arc length normal to the surface. Then, the pertinent equations are multiplied through by $dl = n_r dr + n_z dz$, where n_r and n_z are the r and z components of $\mathbf{n}$, and integrated across the boundary. Integration of the quantity $\frac{\partial F}{\partial r}$, for example, produces the term $n_r < F >$, where the brackets denote the change in the quantity across the boundary. Similarly, the term $\frac{\partial F}{\partial z}$ produces $n_z < F >$. Finally, the main contribution of the partial time derivative of a function F arises from the motion of the boundary, so that integration of the term $\frac{\partial F}{\partial t}$ produces $-\mathbf{v} \cdot \mathbf{n} < F >$, where $\mathbf{v}$ is the velocity of the interface.

Application of the integration procedure to Eq. (1) conserves mass and gives

$$\frac{\partial r_b}{\partial t} + v_z \frac{\partial r_b}{\partial z} = v_r \tag{25}$$

when evaluated at $r = r_b$. The integration of Eq. (2) conserves momentum at the interface and yields

$$n_r p - 2n_r \lambda \frac{\partial v_r}{\partial r} - n_z \lambda \left(\frac{\partial v_r}{\partial z} + \frac{\partial v_z}{\partial r} \right) - \frac{n_r}{2} \left[(B^v)^2 - B^2 \right] = 0 \tag{26}$$

and

$$n_z p - 2n_z \lambda \frac{\partial v_z}{\partial z} - n_r \lambda \left(\frac{\partial v_r}{\partial z} + \frac{\partial v_z}{\partial r} \right) - \frac{n_z}{2} \left[(B^v)^2 - B^2 \right] = 0 \tag{27}$$

at $r = r_b$, where Eqs. (15) - (18) have been substituted for the components of $\Im$. Here the radial and axial components of the unit normal vector $\mathbf{n}$, given by n_r and n_z, are easily defined in terms of the equation of the surface, $r = r_b$. This gives

$$\mathbf{n} = \frac{\nabla(r - r_b)}{|\nabla(r - r_b)|} = \frac{e_r - \frac{\partial r_b}{\partial z} e_z}{\left[1 + \left(\frac{\partial r_b}{\partial z} \right)^2 \right]^{\frac{1}{2}}}, \tag{28}$$

where e_r and e_z are the unit normal vectors in the r and z directions, respectively. Similarly, the integrations of Eqs. (3), (4), and (6) may be performed, but yield either an identity or information which is not required for the analysis. The integration of Eq. (5), however, requires B to be continuous at the interface, or

$$B^v - B = 0 \tag{29}$$

at $r = r_b$. Eqs. (25) - (27) and (29), together with the requirement that v_r, v_z, p and B all remain finite at the centerline, define a complete set of boundary conditions. If the initial conditions are specified, these boundary conditions are sufficient to solve the governing equations in the jet and the vacuum.

3. BASE SOLUTIONS

The unperturbed motion of the jet is characterized by a uniform velocity gradient in the axial direction. This velocity gradient determines both the axial and radial local velocities, as well as the position of the interface at any given time. In addition, a constant axial electric current I is passed through the jet and permitted to diffuse with time. This idealized current distribution induces azimuthal magnetic fields both in the jet and in the surrounding vacuum, which interact to create Lorentz forces. These electromagnetic forces, as well as inertial forces which arise from the velocity gradients, affect the idealized stress distribution in the jet.

The unperturbed velocities and radius of the jet have been presented many times (Powell and Littlefield 1990; Curtis 1987; Pack 1988; Romero 1989; Littlefield and Powell 1990), but will be repeated here for convenience. The subscript zero will be used to denote these idealized quantities. The axial and radial velocities are given by

$$v_{z0} = \frac{\eta z}{\tau} \tag{30}$$

and

$$v_{r0} = -\frac{\eta r}{2\tau}, \tag{31}$$

where η is the initial strain rate and $\tau = 1 + \eta t$. This velocity distribution requires the unperturbed value of λ to be $\lambda_0 = Y\tau/3\eta$. The radius at the boundary is given by

$$r_{b0} = \frac{a}{\tau^{1/2}}, \tag{32}$$

where a is the initial radius of the jet. The magnetic field and stress profiles depend on these velocities, and on the current distribution in the jet. The magnetic-induction field in the vacuum, for example, is required by Ampère's Law to be

$$B_0^v = \frac{\mu_0 I}{2\pi r}, \tag{33}$$

which also satisfies Eq. (24). The zero-order pressure distribution in the jet is determined from the integration of Eq. (21) which, after substitution of the velocities given in Eqs. (30) and (31) and use of the boundary condition in Eq. (26), yields

$$p_0 = \frac{3\rho\eta^2}{8\tau^3}(a^2 - \tau r^2) - \frac{Y}{3} + \frac{1}{\mu_0}\int_r^{r_\infty} \frac{B_0(u,\tau)}{u}\frac{\partial}{\partial u}[uB_0(u,\tau)]du, \tag{34}$$

where B_0 is the zero-order magnetic field in the jet.

This magnetic field must satisfy Eq. (23), which may be simplified to yield

$$\frac{\partial B_0}{\partial t} - \frac{\eta r}{2\tau}\frac{\partial B_0}{\partial r} + \frac{\eta B_0}{2\tau} = \frac{1}{\sigma\mu_0}\left(\frac{\partial^2 B_0}{\partial r^2} + \frac{1}{r}\frac{\partial B_0}{\partial r} - \frac{B_0}{r^2}\right). \tag{35}$$

The advection term in Eq. (35) may be completely eliminated by a coordinate transformation which deforms in accordance with the stretching motion of the jet, together with a transformation for B_0. A suitable transformation may be defined as

$$\tilde{z} = \frac{z}{a\tau}, \quad \tilde{r} = \frac{r\tau^{1/2}}{a}, \quad \tau = 1 + \eta t, \quad \hat{B}_0 = \tau^{1/2} B_0 \tag{36}$$

which, when substituted into Eq. (35), yields

$$\frac{\partial \hat{B}_0}{\partial \tau} = \frac{\tau}{R}\left(\frac{\partial^2 \hat{B}_0}{\partial \tilde{r}^2} + \frac{1}{\tilde{r}}\frac{\partial \hat{B}_0}{\partial \tilde{r}} - \frac{\hat{B}_0}{\tilde{r}^2}\right), \tag{37}$$

where $R = \sigma\mu_0\eta a^2$ is the magnetic Reynolds number. The boundary condition in Eq. (29) requires B_0 to be continuous at the interface, which gives

$$\hat{B}_0 = \frac{\mu_0 I \tau}{2\pi a} \tag{38}$$

at $\tilde{r} = 1$. The specific solution for $\hat{B}_0$ depends on the initial condition chosen. In the present analysis, two different cases are considered for this condition: an initial surface current and an initial body current.

3.1 Initial Surface Current. If the current is initially located on the surface of the jet, the appropriate initial condition is $\hat{B}_0 = 0$ at $\tau = 1$. Moreover, since the boundary condition given in Eq. (38) is time dependent, Duhamel's theorem (Carslaw and Jaeger 1959) must be employed to find a solution to Eq. (37). Application of the theorem requires the solution to an auxiliary problem for $\hat{B}_0^a$. The governing differential equation for $\hat{B}_0^a$ is identical to the equation for $\hat{B}_0$, but the boundary condition is given by

$$\hat{B}_0^a = \frac{\mu_0 I \bar{\tau}}{2\pi a} \tag{39}$$

at $\tilde{r} = 1$, where $\bar{\tau}$ is treated as a constant. The solution to this auxiliary problem is given by

$$\tilde{B}_0^a(\tilde{r}, \tau, \bar{\tau}) = \bar{\tau}\tilde{r} + \sum_{j=0}^{\infty} \frac{2\bar{\tau} J_1(\gamma_j \tilde{r})}{\gamma_j J_0(\gamma_j)} \exp\left[-\frac{\gamma_j^2}{2R}(\tau^2 - 1)\right], \tag{40}$$

where J_0 and J_1 are Bessel functions, $\tilde{B}_0^a = \frac{2\pi a \hat{B}_0^a}{\mu_0 I}$, and γ_j satisfies the transcendental equation $J_1(\gamma_j) = 0$. This solution is then used in Duhamel's integral to find a solution for $\hat{B}_0$, which gives

$$\hat{B}_0(\tilde{r}, \tau) = \frac{1}{\tau}\frac{\partial}{\partial \tau}\int_1^{\tau} \bar{\tau} \hat{B}_0^a[\tilde{r}, (\tau^2 - \bar{\tau}^2 + 1)^{1/2}, \bar{\tau}] d\bar{\tau}$$

$$= \frac{\mu_0 I}{2\pi a}\left(\tau\tilde{r} + \sum_{j=0}^{\infty} \frac{2J_1(\gamma_j \tilde{r})}{\gamma_j J_0(\gamma_j)}\left\{e^{\omega_j^2(1-\tau^2)} + \frac{1}{\omega_j}\left[D(\omega_j \tau) - e^{\omega_j^2(1-\tau^2)} D(\omega_j)\right]\right\}\right), \tag{41}$$

where ω_j is defined as $\omega_j = \gamma_j/(2R)^{1/2}$, and D is Dawson's integral (Abramowitz and Stegun 1964). In Fig. 2, the dimensionless magnetic field $\tilde{B}_0$ is plotted vs. $\tilde{r}$ at several times for a magnetic Reynolds number of ten, where $\tilde{B}_0 = \frac{2\pi a \hat{B}_0}{\mu_0 I \tau^{1/2}}$. As is evident from the figure, the current is initially concentrated at the surface, then diffuses to the interior of the jet as time progresses. Apparently, for this magnetic Reynolds number the current is almost completely diffused when $\tau = 2$. Also, the magnetic field at the surface increases with time, due to the decrease in the cross sectional area associated with the stretching motion of the jet. Evidently, this increase in $\tilde{B}_0$ always prevents the current from ever diffusing completely.

3.2 Initial Body Current. When the electrical current is completely diffused initially, the appropriate initial condition on $\hat{B}_0$ is

$$\hat{B}_0 = \frac{\mu_0 I \tilde{r}}{2\pi a} \tag{42}$$

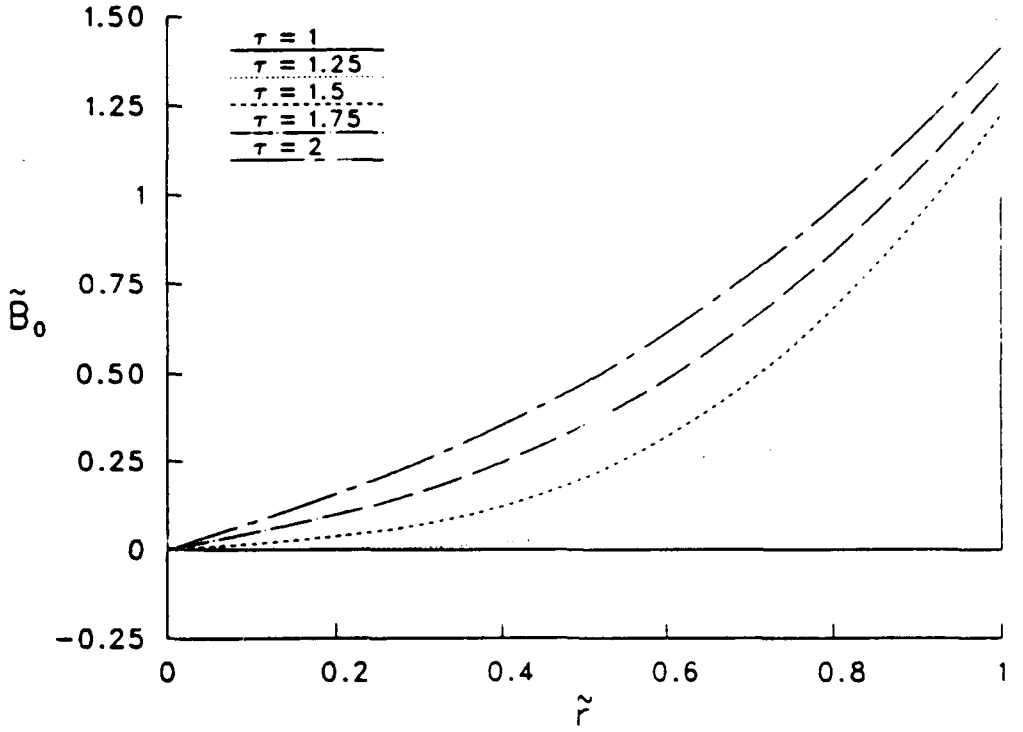

Figure 2. $\tilde{B}_0$ versus $\tilde{r}$ at several times for $R = 10$, assuming an initial surface current.

at $\tau = 1$. Application of this condition to Eq. (37), using a solution procedure similar to the initial surface current case presented above, gives

$$\hat{B}_0 = \frac{\mu_0 I}{2\pi a}\left(\tau\tilde{r} + \sum_{j=0}^{\infty} \frac{2J_1(\gamma_j\tilde{r})}{\gamma_j\omega_j J_0(\gamma_j)}\left[D(\omega_j\tau) - e^{\omega_j^2(1-\tau^2)}D(\omega_j)\right]\right). \tag{43}$$

Fig. 3 shows $\tilde{B}_0$ vs. $\tilde{r}$ at several times for $R = 10$, where $\tilde{B}_0 = \frac{2\pi a\hat{B}_0}{\mu_0 I\tau^{1/2}}$. Apparently, for this magnetic Reynolds number the electric current remains almost completely diffused at all times. The positive curvature in the profiles for $\tilde{B}_0$ are indicative of only slight current diffusion towards the centerline of the jet. The slight decrease in $\tilde{B}_0$ at early times in the jet interior is an advection effect associated with the stretching motion.

4. PERTURBATION EQUATIONS

To study the stability of the idealized stretching motion presented in Sec. 3, a small disturbance is introduced to the flow and permitted to develop over time. The equations which govern the time evolution of this disturbance are formulated using linear perturbation theory, for which solutions are valid provided the overall magnitudes of the disturbances remain small.

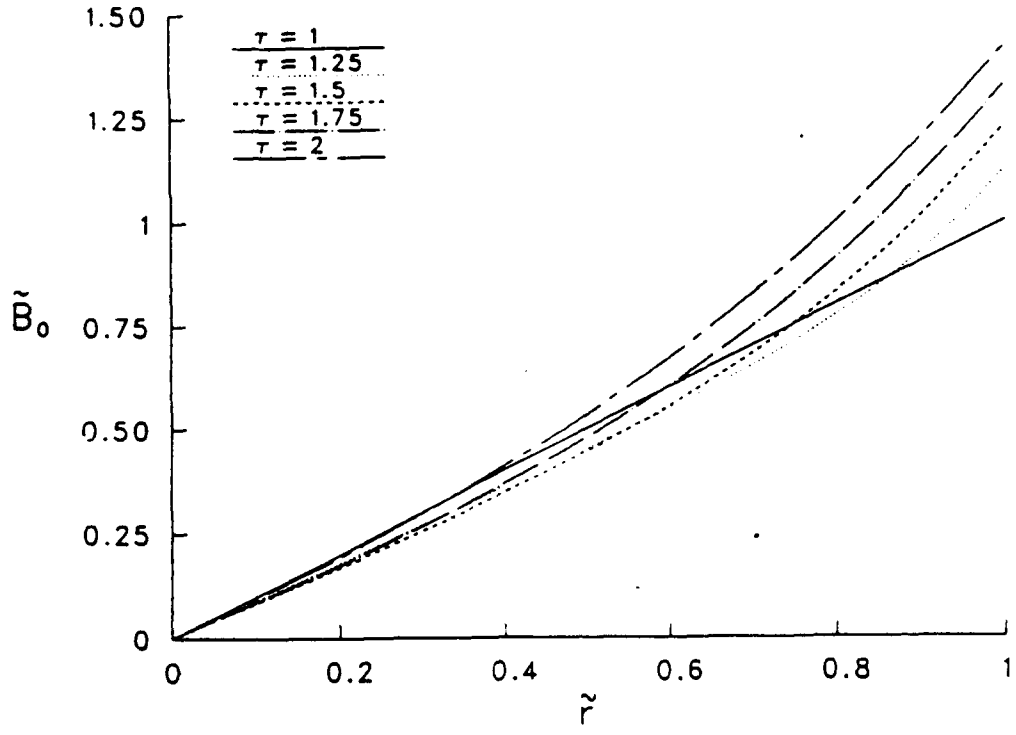

Figure 3. $\tilde{B}_0$ versus $\tilde{r}$ at several times for $R = 10$, assuming an initial body current.

The development of the perturbation equations is accomplished through the substitution of the variables

$$\begin{aligned} v_r &= v_{r0} + v_{r1}, \quad v_z = v_{z0} + v_{z1}, \\ \lambda &= \lambda_0 + \lambda_1, \quad p = p_0 + p_1, \\ B &= B_0 + B_1, \quad B^v = B_0^v + B_1^v, \\ r_b &= r_{b0} + r_{b1}, \end{aligned} \tag{44}$$

into the governing differential equations, where the subscript one denotes a first order quantity. Keeping terms which are of zero- and first-order only, and recognizing the zero order solutions also satisfy the governing equations, the continuity equation gives

$$\frac{\partial v_{r1}}{\partial r} + \frac{v_{r1}}{r} + \frac{\partial v_{z1}}{\partial z} = 0. \tag{45}$$

Similarly, the scalar forms of the momentum equation yield

$$\rho\left(\frac{\partial v_{r1}}{\partial t}-\frac{\eta v_{r1}}{2\tau}-\frac{\eta r}{2\tau}\frac{\partial v_{r1}}{\partial r}+\frac{\eta z}{\tau}\frac{\partial v_{r1}}{\partial z}\right)=\frac{\partial p_1}{\partial r}+\lambda_0\frac{\partial^2 v_{r1}}{\partial z^2}$$

$$-\frac{1}{\mu_0}\left[B_0\frac{\partial B_1}{\partial r}+\left(\frac{\partial B_0}{\partial r}+\frac{2B_0}{r}\right)B_1\right] \tag{46}$$

and

$$\rho\left(\frac{\partial v_{z1}}{\partial t}+\frac{\eta v_{z1}}{\tau}-\frac{\eta r}{2\tau}\frac{\partial v_{z1}}{\partial r}+\frac{\eta z}{\tau}\frac{\partial v_{z1}}{\partial z}\right)=\frac{\partial p_1}{\partial z}+\lambda_0\left(\frac{\partial^2 v_{z1}}{\partial r^2}+\frac{1}{r}\frac{\partial v_{z1}}{\partial r}-\frac{\partial^2 v_{z1}}{\partial z^2}\right)$$

$$-\frac{B_0}{\mu_0}\frac{\partial B_1}{\partial z}, \tag{47}$$

where substitution of the zero-order velocities given in Sec. 3 has been performed, and λ_1 has been eliminated using the relation

$$\lambda_1=-\frac{\tau}{\eta}\frac{\partial v_{z1}}{\partial z}\lambda_0. \tag{48}$$

Eq. (48) represents the first order contributions to Eq. (20). The magnetic convection-diffusion equation yields

$$\frac{\partial B_1}{\partial t}+\frac{\eta B_1}{2\tau}+\left(\frac{\partial B_0}{\partial r}-\frac{B_0}{r}\right)v_{r1}-\frac{\eta r}{2\tau}\frac{\partial B_1}{\partial r}+\frac{\eta z}{\tau}\frac{\partial B_1}{\partial z}=\frac{1}{\sigma\mu_0}\left(\frac{\partial^2 B_1}{\partial r^2}+\frac{1}{r}\frac{\partial B_1}{\partial r}-\frac{B_1}{r^2}+\frac{\partial^2 B_1}{\partial z^2}\right). \tag{49}$$

It is advantageous to simplify Eqs. (45) - (49) further before solving them. The result of a previous analysis (Romero 1989) has demonstrated a coordinate transformation which deforms in accordance with the stretching motion of the jet, given by

$$\tilde{z}=\frac{z}{a\tau},\quad \tilde{r}=\frac{r\tau^{1/2}}{a},\quad \tau=1+\eta t, \tag{50}$$

eliminates the explicit z dependence in the perturbation equations. This permits the axial dependence of the independent variables to be Fourier analyzed, which facilitates the calculations. Furthermore, the number of independent parameters in the problem may be minimized if the perturbation equations are cast in dimensionless form. Let

$$v_{r1} = \eta a \tilde{v}_r \exp(ik\tilde{z}), \quad v_{z1} = \eta a \tilde{v}_z \exp(ik\tilde{z}),$$

$$\lambda_1 = \frac{Y}{\eta}\tilde{\lambda}\exp(ik\tilde{z}), \quad p_1 = \rho\eta^2 a^2 \tilde{p}\exp(ik\tilde{z}),$$

$$B_1 = \frac{\mu_0 I}{2\pi a}\tilde{B}\exp(ik\tilde{z}), \quad B_1^v = \frac{\mu_0 I}{2\pi a}\tilde{B}^v\exp(ik\tilde{z}),$$

$$r_{b1} = r_{b0}\tilde{r}_b\exp(ik\tilde{z}), \tag{51}$$

where k is the axial wavenumber and $i = \sqrt{-1}$. Then the perturbation equations for the dimensionless velocity, pressure and magnetic field in the jet may be derived from Eqs. (45) - (49), and are given by

$$\frac{\partial \tilde{v}_r}{\partial \tilde{r}} + \frac{\tilde{v}_r}{\tilde{r}} + \frac{ik}{\tau^{3/2}}\tilde{v}_z = 0, \tag{52}$$

$$\tau\frac{\partial \tilde{v}_r}{\partial \tau} - \frac{\tilde{v}_r}{2} = -\tau^{3/2}\frac{\partial \tilde{p}}{\partial \tilde{r}} - \frac{k^2}{\Omega}\tilde{v}_r - \Lambda\tau^{3/2}\left[\tilde{B}_0\frac{\partial \tilde{B}}{\partial \tilde{r}} + \left(\frac{\partial \tilde{B}_0}{\partial \tilde{r}} + \frac{2\tilde{B}_0}{\tilde{r}}\right)\tilde{B}\right], \tag{53}$$

$$\tau\frac{\partial \tilde{v}_z}{\partial \tau} + \tilde{v}_z = -ik\tilde{p} + \frac{\tau^3}{\Omega}\left(\frac{\partial^2 \tilde{v}_z}{\partial \tilde{r}^2} + \frac{1}{\tilde{r}}\frac{\partial \tilde{v}_z}{\partial \tilde{r}} + \frac{k^2}{\tau^3}\tilde{v}_z\right) - ik\Lambda\tilde{B}_0\tilde{B}, \tag{54}$$

and

$$\frac{\partial \tilde{B}}{\partial \tau} + \frac{\tilde{B}}{2\tau} + \tau^{1/2}\left(\frac{\partial \tilde{B}_0}{\partial \tilde{r}} - \frac{\tilde{B}_0}{\tilde{r}}\right)\tilde{v}_r = \frac{\tau}{R}\left(\frac{\partial^2 \tilde{B}}{\partial \tilde{r}^2} + \frac{1}{\tilde{r}}\frac{\partial \tilde{B}}{\partial \tilde{r}} - \frac{\tilde{B}}{\tilde{r}^2} - \frac{k^2}{\tau^3}\tilde{B}\right). \tag{55}$$

Here the dimensionless parameters Ω and Λ are defined by

$$\Omega = \frac{3\rho\eta^2 a^2}{Y}; \quad \Lambda = \frac{\mu_0 I^2}{4\pi^2\rho\eta^2 a^4}, \tag{56}$$

and R is the magnetic Reynolds number. Ω and Λ physically represent the relative magnitudes of inertial to plastic forces, and electromagnetic to inertial forces, respectively; and R is a ratio of magnetic convection to diffusion.

In the vacuum surrounding the jet, previous analysis (Littlefield and Powell 1990) has demonstrated that the perturbed magnetic field, $\tilde{B}^v$, is identically zero. This result also

follows directly from Ampère's Law, since the total current in the jet remains constant over time.

The boundary conditions applicable at the interface between the jet and the vacuum must also be specified, and may be derived from Eqs. (25) - (29). The first order contributions to these conditions are evaluated, keeping in mind that the zero order contributions are identically satisfied by the zero order solutions. Furthermore, the first order contribution of the zero order solutions evaluated at the perturbed boundary must also be included. For example, the first order contributions to the condition $F = 0$ would be determined as

$$F_1 + \left.\frac{\partial F_0}{\partial r}\right|_{r=r_{b0}} r_{b1} = 0, \tag{57}$$

evaluated at $r = r_{b0}$. Consequently, the boundary condition on $\tilde{B}$, which is derived from Eq. (29), is given by

$$\tilde{B} + \left(\tau^{1/2} + \frac{\partial \tilde{B}_0}{\partial \tilde{r}}\right)\tilde{r}_b = 0, \tag{58}$$

evaluated at $\tilde{r} = 1$. Here the appropriate dimensionless variables have been used, and the axial dependence has been Fourier analyzed. The remaining boundary conditions are determined from Eqs. (25) - (28), and are given by

$$\tilde{p} - \left(\frac{3}{4\tau^3} + \Lambda\left[\tau^{1/2} + \frac{\partial \tilde{B}_0}{\partial \tilde{r}}\right]\right)\tilde{r}_b - \frac{\tau^{3/2}}{\Omega}\left(2\frac{\partial \tilde{v}_r}{\partial \tilde{r}} + \frac{ik}{\tau^{3/2}}\tilde{v}_z\right) = 0, \tag{59}$$

$$3ik\tilde{r}_b - ik\tau^{3/2}\tilde{v}_r - \tau^3\frac{\partial \tilde{v}_z}{\partial \tilde{r}} = 0 \tag{60}$$

and

$$\frac{\partial \tilde{r}_b}{\partial \tau} - \tau^{1/2}\tilde{v}_r = 0, \tag{61}$$

when evaluated at $\tilde{r} = 1$.

A suitable set of initial conditions must also be specified before the perturbation equations can be solved. In the present analysis, the initial amplitude of the perturbed axial velocity, $\tilde{v}_z$, was assumed constant. This gives

$$\tilde{v}_z = iC, \tag{62}$$

where C is real. This specification satisfies the conditions at the axis and, apparently, is sufficient to determine the initial conditions on most of the remaining variables. Eq. (52) requires the perturbed radial velocity to be

$$\tilde{v}_r = \frac{kC\tilde{r}}{2}, \tag{63}$$

and Eq. (61) yields

$$\tilde{r}_b = \frac{kC}{6} \tag{64}$$

for the perturbed radius. The initial condition for the perturbed magnetic field is different, depending on the solution specified for $\tilde{B}_0$. For the initial surface current case, $\tilde{B}$ was assumed zero, and for the initial body current case, $\tilde{B}$ was assumed to be a linear function of $\tilde{r}$. This gives

$$\tilde{B} = -\frac{kC\tilde{r}}{3} \tag{65}$$

for the initial body current case. The first-order pressure satisfies a Poisson-type equation, which is formulated from the time derivative of the continuity equation. The solution for $\tilde{p}$ is different depending on the solution chosen for $\tilde{B}$. For the initial surface current case, $\tilde{p}$ is given by

$$\tilde{p} = C_1 I_0(k\tilde{r}) - C\frac{3\Omega - 2k^2}{k\Omega}, \tag{66}$$

where I_0 is a modified Bessel function and

$$C_1 = \left[\frac{3\Omega - 2k^2}{k\Omega} + \left(\frac{3}{4} - \Lambda\right)\tilde{r}_b\right]\frac{C}{I_0(k)}. \tag{67}$$

For the initial body current case, $\tilde{p}$ is given by

$$\tilde{p} = \frac{\Lambda(4 - k^2\tilde{r}^2)C}{3k} + \frac{(2k^2 - 3\Omega)C}{\Omega k} + C_2 I_0(k\tilde{r}) \tag{68}$$

where

$$C_2 = \left[\frac{k}{8} - \frac{2\Lambda(2-k^2)}{3k} - \frac{2k^2-3\Omega}{\Omega k}\right] \frac{\cdot}{I_0(k)}. \tag{69}$$

The constant C is arbitrary and was chosen as $C = \frac{6}{k}$ so that $\tilde{r}_b = 1$ initially. Using these initial conditions, Eqs. (52) - (55), together with the boundary conditions in Eqs. (58) - (61), may be solved for the five unknowns in the jet: $\tilde{v}_r$, $\tilde{v}_z$, $\tilde{p}$, $\tilde{B}$, and $\tilde{r}_b$.

5. SOLUTION TO PERTURBATION EQUATIONS AND DISCUSSION

Once solutions to the perturbation equations are obtained, they may be used to identify disturbances that are unstable. A particular disturbance is considered unstable if it grows in an unbounded manner as time progresses. Since it is not practical to monitor the solutions of every dependent variable when a disturbance is introduced, the growth rate of a single variable is often used to determine the stability criterion. Fortunately, the selection of this variable is usually not very critical, because it is often obvious when a particular disturbance is unstable. In the present analysis, the relative perturbed amplitude, $\tilde{r}_b$, is monitored to establish the stability criterion. If $|\tilde{r}_b|$ grows with time, the disturbance is identified as unstable.

The numerical integration of Eqs. (52) - (55) may be accomplished in a straightforward manner using standard finite difference techniques. A radially implicit scheme second order in $\tilde{r}$ and first order in τ was employed. Although the application of this scheme proved to be satisfactory in most respects, calculations of sufficient accuracy were sometimes difficult to obtain. Apparently, there were two major causes for this loss in accuracy. First, the numerical evaluation of the infinite series in $\tilde{B}_0$, as given by Eqs. (41) and (43), often resulted in large truncation errors, particularly at early times. Consequently, it was sometimes necessary to approximate $\tilde{B}_0$ by direct numerical integration of Eq. (37). Second, the numerical evaluation of $\tilde{B}$ was often inaccurate at early times due to the near-discontinuity in its slope near the boundary. As a result, very small times steps were sometimes required to obtain accurate solutions.

The result of a calculation for $\tilde{r}_b$, using the initial conditions for the initial surface current case, is depicted in Fig. 4. The relative amplitude is shown vs. $\tilde{t}$, where $\tilde{t} = \eta t$. The parameters Ω and Λ were taken to be one, and the magnetic Reynolds number was taken as ten. Several curves are shown for various values for the wavenumber k. which is related to the wavelength of the perturbation at any given time by $\lambda_w = \frac{2\pi\tau a}{k}$. As is evident from the figure, disturbances of all wavelengths appear to be unstable. The most unstable dis-

turbance at early times has an initial wavelength approximately equal to the jet diameter, corresponding to $k = \pi$. At later times, the slopes in the curves for the shorter wavelength disturbances increase, indicating an increase in growth rate for these perturbations. Presumably, this increase would eventually result in larger relative amplitudes for the initially shorter wavelength disturbances. These observations are in qualitative agreement with the instabilities found in perfectly conducting jets (Littlefield and Powell 1990).

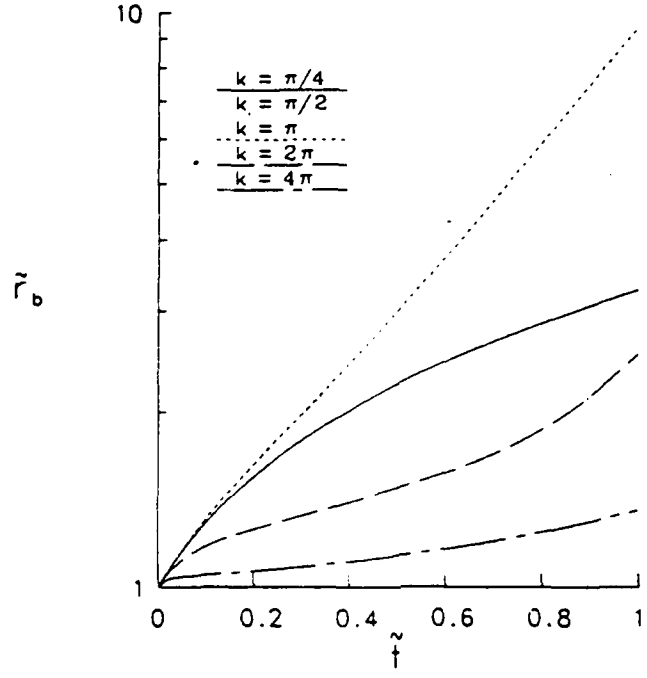

Figure 4. Relative amplitude $\tilde{r}_b$ versus dimensionless time for different values of k with $\Omega = \Lambda = 1$ and $R = 10$, assuming an initial surface current.

If the initial current distribution corresponds to a uniform body current, a similar result is obtained for the relative amplitude. In Fig. 5 the relative amplitude is shown vs. $\tilde{t}$, assuming an initial body current, using the same parameters previously specified in Fig. 4. A comparison of Fig. 4 with Fig. 5 reveals virtually identical behavior in the growth of $\tilde{r}_b$. This is a surprising result considering the major differences in current distribution for the two cases, as indicated in Figs. 2 and 3. Apparently, a change in the current distribution has only a minor effect on the growth rate of the relative amplitude.

To assess the overall effect of electrical conductivity on the growth rate of perturbations, the relative amplitude $\tilde{r}_b$ is plotted in Fig. 6 vs. $\tilde{t}$ for three different magnetic Reynolds numbers. The parameters Ω and Λ were taken as one, and the wavenumber k was taken as π, which corresponds to the most unstable wavelength in all cases. Evidently, the largest growth rate in $\tilde{r}_b$ is observed when the electrical conductivity is very large, corresponding to

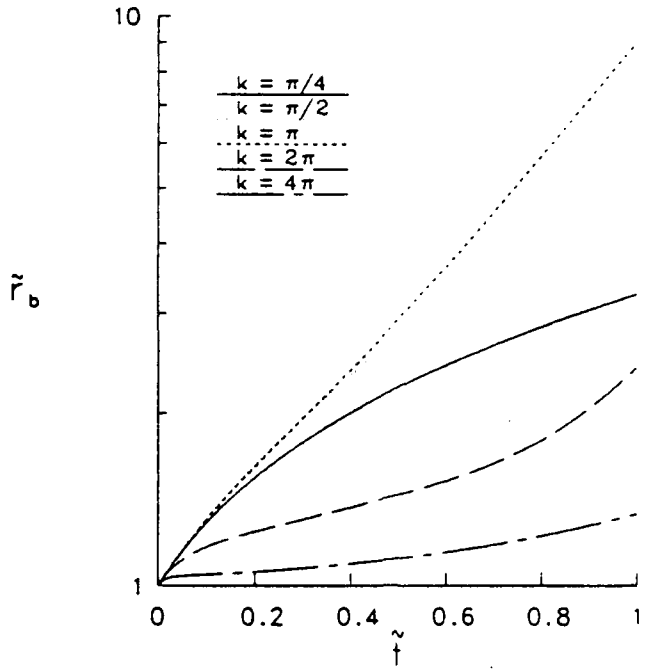

Figure 5. Relative amplitude $\tilde{r}_b$ versus dimensionless time for different values of k with $\Omega = \Lambda = 1$ and $R = 10$, assuming an initial body current.

$R \to \infty$. The smallest growth rate in relative amplitude occurs in the absence of electrical current, or when $R = 0$. When $R = 10$, the range in $\tilde{r}_b$ falls between these two extremes, but is reasonably close to the values for $R \to \infty$. An increase in the electrical conductivity, apparently, results in only small increases in the relative amplitude.

The physical mechanisms responsible for the hydrodynamic and MHD instabilities found in jets have been discussed in detail elsewhere (Powell and Littlefield 1990; Littlefield and Powell 1990) for jets of infinite conductivity. Evidently, the same physical mechanisms are also applicable to jets of finite conductivity, and result in the same qualitative conclusions about the stability. In particular, the application of electrical current to a perturbed jet results in variations in the magnetic field and current density, which both increase in regions where localized necking occurs. The current and magnetic field interact to create Lorentz forces that always decrease the stability of the jet. The exact location and magnitude of these Lorentz forces depends on many factors, including the assumption for electrical conductivity. If infinite conductivity is assumed, for example, the Lorentz forces are concentrated at the surface of the jet. For jets of finite conductivity, however, the Lorentz forces are distributed throughout the cross section.

Disturbances in the current clearly result in decreases of the stability of jets. A qualitative discussion of the Lorentz forces, however, does not sufficiently explain the differences in

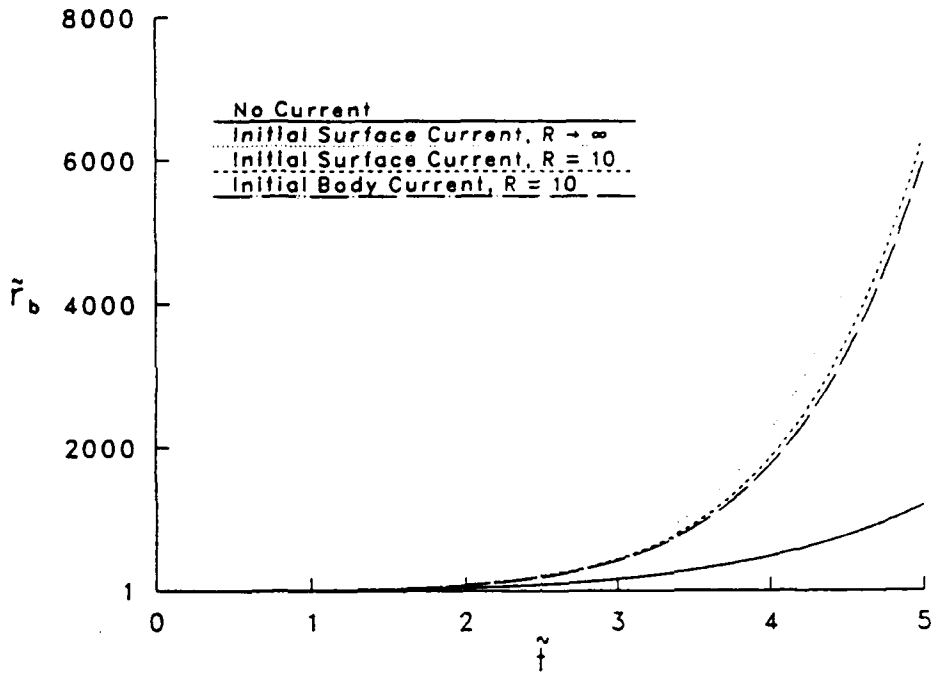

Figure 6. Comparison of relative amplitudes at different times when $R \to \infty$, $R = 10$ and $R = 0$, with $\Omega = \Lambda = 1$ and $k = \pi$.

relative amplitude depicted in Fig. 6. It is necessary to understand the effect of current distribution on the magnitude of the Lorentz forces. A convenient method for making objective comparisons is to consider the net axial Lorentz force per unit length on a differential disk of width dz in the jet. It is this force that causes the disk to be accelerated out of the neck. A simple computation reveals this force is initially given by

$$F = \frac{ik^2 C \mu_0 I^2}{24\pi a} \exp(ik\tilde{z}) \tag{70}$$

if the current is concentrated at the surface. For a uniform body current, the axial force per unit volume is initially given by

$$f = \frac{ik^2 C \mu_0 I^2 r^2}{12\pi^2 a^5} \exp(ik\tilde{z}) \tag{71}$$

which, when integrated over the area of the disk, gives the result in Eq. (70). At later times, initial surface currents remain on the surface for $\sigma \to \infty$, and uniform body currents remain relatively uniform for finite conductivity. As a consequence, the axial Lorentz forces, as well as the relative amplitude, should remain approximately equal at later times for the different current distributions. The infinite conductivity case, apparently, results in only slightly higher growth rates for $\tilde{r}_b$, because the Lorentz forces are concentrated on the surface of

the jet. This concentration of forces slightly increases the velocities at the surface, which increases the relative amplitude.

The effect of current distribution on the Lorentz forces in the jet becomes readily apparent upon examination of the velocity disturbances. In Fig. 7, the perturbation streamlines are shown for a wavelength segment of the jet at time $\tilde{t} = 0.5$, where $\Omega = \Lambda = 1$, $R = 10$, and $k = 3\pi/2$. The left portion of the figure shows the streamlines for an initial surface current, whereas the right portion corresponds to an initial body current. In both figures, a stabilizing secondary motion is observed in the central portion of the jet. This secondary motion is apparently caused by restoring plastic forces in the jet (Littlefield and Powell 1990) and is present even in the absence of electromagnetic effects. The initial body current case, however, displays an additional cell near the centerline of the jet. Evidently, the presence of this cell is caused by electromagnetic body forces that act near the centerline when current is distributed uniformly throughout the jet. Even though the perturbation in the boundary appears to be equal in both cases, the disturbance velocity distributions are quite different.

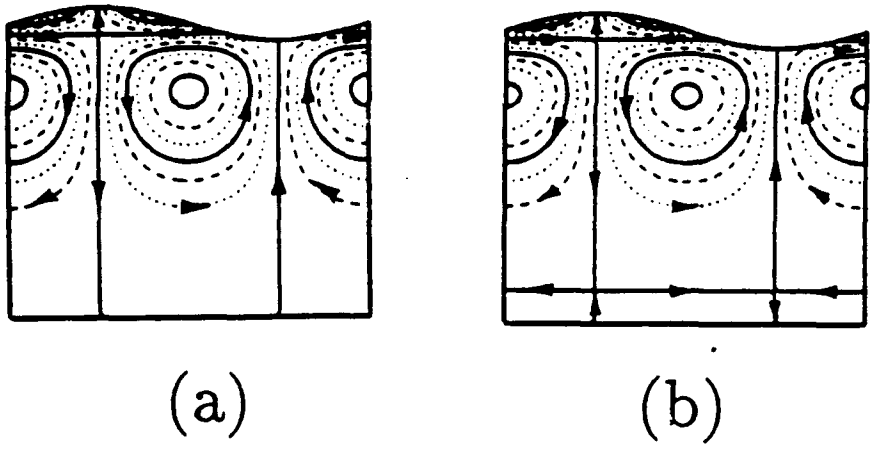

Figure 7. Perturbation velocity streamlines for a wavelength segment of the jet at $\tilde{t} = 0.5$ with $k = 3\pi/2$, $\Omega = \Lambda = 1$ and $R = 10$ for (a) an initial surface current and (b) an initial body current.

6. CONCLUSIONS

The overall effect of finite electrical conductivity on the stability of uniformly elongating plastic jets appears to be mostly quantitative. The largest growth rates in the boundary perturbation are observed for jets of infinite conductivity; the magnitude in $\tilde{r}_b$ for jets of finite conductivity differs only slightly from these results. These similarities, however, are not totally unexpected. The electrical current was assumed equal in every case and, consequently the average magnetic pressure in the jet is about the same for all conductivities. The local value for the pressure, however, is variable and depends on the current distribution in the jet, as well as the conductivity. Apparently, the small differences in $\tilde{r}_b$ result from small local variations in the magnetic pressure. This pressure becomes concentrated at the surface for large conductivities which, evidently, results in slightly larger growth rates for $\tilde{r}_b$.

Application of the analysis to shaped-charge jets indicates that electrical currents significantly increase the instabilities in the jets and may reduce the breakup time. Calculations for realistic levels of electrical conductivity do not appreciably alter this result. The increase in instability is present even for sufficiently low current levels, where large scale changes in the density and temperature of the jet are not expected.

7. REFERENCES

Abramowitz, M. and Stegun, I. A. *Handbook of Mathematical Functions.* Washington, DC: US Government Printing Office, 1964, p.298.

Carslaw, H. S. and Jaeger, J. C. *Conduction of Heat in Solids.* London: Clarendon Press, 1959, p. 30.

Curtis, J. P. "Axisymmetric Instability Model for Shaped Charge Jets." *Journal of Applied Physics*, vol. 61, no. 11, pp. 4978-4985, June 1987.

Kruskal, M. and Schwartzschild, M. "Some Instabilities of a Completely Ionized Plasma." *Proceedings Royal Society of London*, vol. A223, pp. 348-360, 1954.

Littlefield, D. L. and Powell, J. D. "The Effect of Electromagnetic Fields on the Stability of a Uniformly Elongating Plastic Jet." *Physics of Fluids A*, vol. 2, no. 12, pp. 2240-2248, December 1990.

Pack, D. C. "On the Perturbation and Break Up of a High-Speed, Elongating Metal Jet." *Journal of Applied Physics*, vol. 19, no. 6, pp. 1864-1871, March 1988.

Powell, J. D., and Littlefield, D. L. "Effect of Electromagnetic Fields on the Stability of a Perfectly Conducting, Axisymmetric Shaped-Charge Jet." BRL-TR-3108, U. S. Army Ballistic Research Laboratory, Aberdeen Proving Ground, MD, June 1990.

Romero, L. A. "The Instability of Rapidly Stretching Plastic Jets. *Journal of Applied Physics*, vol. 65, no. 8. pp. 3006-3016, April 1989.

Tayler, R. J. "Hydromagnetic Instabilities of an Ideally Conducting Fluid." *Proceedings of the Physical Society*, vol. 70, pp. 31-49, 1956.

INTENTIONALLY LEFT BLANK.

No. of Copies	Organization
2	Administrator Defense Technical Info Center ATTN: DTIC-DDA Cameron Station Alexandria, VA 22304-6145
1	Commander U.S. Army Materiel Command ATTN: AMCAM 5001 Eisenhower Avenue Alexandria, VA 22333-0001
1	Commander U.S. Army Laboratory Command ATTN: AMSLC-DL 2800 Powder Mill Road Adelphi, MD 20783-1145
2	Commander U.S. Army Armament Research, Development, and Engineering Center ATTN: SMCAR-IMI-I Picatinny Arsenal, NJ 07806-5000
2	Commander U.S. Army Armament Research, Development, and Engineering Center ATTN: SMCAR-TDC Picatinny Arsenal, NJ 07806-5000
1	Director Benet Weapons Laboratory U.S. Army Armament Research, Development, and Engineering Center ATTN: SMCAR-CCB-TL Watervliet, NY 12189-4050
(Unclass. only) 1	Commander U.S. Army Armament, Munitions and Chemical Command ATTN: AMSMC-IMF-L Rock Island, IL 61299-5000
1	Director U.S. Army Aviation Research and Technology Activity ATTN: SAVRT-R (Library) M/S 219-3 Ames Research Center Moffett Field, CA 94035-1000

No. of Copies	Organization
1	Commander U.S. Army Missile Command ATTN: AMSMI-RD-CS-R (DOC) Redstone Arsenal, AL 35898-5010
1	Commander U.S. Army Tank-Automotive Command ATTN: ASQNC-TAC-DIT (Technical Information Center) Warren, MI 48397-5000
1	Director U.S. Army TRADOC Analysis Command ATTN: ATRC-WSR White Sands Missile Range, NM 88002-5502
1	Commandant U.S. Army Field Artillery School ATTN: ATSF-CSI Ft. Sill, OK 73503-5000
(Class. only) 1	Commandant U.S. Army Infantry School ATTN: ATSH-CD (Security Mgr.) Fort Benning, GA 31905-5660
(Unclass. only) 1	Commandant U.S. Army Infantry School ATTN: ATSH-CD-CSO-OR Fort Benning, GA 31905-5660
1	Air Force Armament Laboratory ATTN: WL/MNOI Eglin AFB, FL 32542-5000
	Aberdeen Proving Ground
2	Dir, USAMSAA ATTN: AMXSY-D AMXSY-MP, H. Cohen
1	Cdr, USATECOM ATTN: AMSTE-TC
3	Cdr, CRDEC, AMCCOM ATTN: SMCCR-RSP-A SMCCR-MU SMCCR-MSI
1	Dir, VLAMO ATTN: AMSLC-VL-D
10	Dir, BRL ATTN: SLCBR-DD-T

No. of
Copies Organization

1 Orlando Technologies, Incorporated
ATTN: Dr. Daniel A. Matuska
P.O. Box 855
Shalimar, FL 32579

2 Science Applications International Corporation
ATTN: Dr. Jad H. Batteh
Mr. Lindsey Thornhill
1503 Johnson Ferry Road
Marietta, GA 30062

2 Science Applications International Corporation
ATTN: Dr. Keith A. Jamison
Dr. Glenn E. Rolader
1247-B North Eglin Parkway
Shalimar, FL 32579

1 Science Applications International Corporation
ATTN: Dr. A.J. Toepfer
2109 Air Park Road, S.E.
Albuquerque, NM 87122

1 TITAN Spectron Division
ATTN: Dr. Bruce R. Miller
2340 Alamo Boulevard, S.E.
Suite 200
Albuquerque, NM 87106

1 Georgia Institute of Technology
ATTN: Dr. P.V. Desai
Department of Mechanical Engineering
Atlanta, GA 30332

USER EVALUATION SHEET/CHANGE OF ADDRESS

This laboratory undertakes a continuing effort to improve the quality of the reports it publishes. Your comments/answers below will aid us in our efforts.

1. Does this report satisfy a need? (Comment on purpose, related project, or other area of interest for which the report will be used.) _____

_____

_____

2. How, specifically, is the report being used? (Information source, design data, procedure, source of ideas, etc.) _____

_____

_____

3. Has the information in this report led to any quantitative savings as far as man-hours or dollars saved, operating costs avoided, or efficiencies achieved, etc? If so, please elaborate. _____

_____

_____

4. General Comments. What do you think should be changed to improve future reports? (Indicate changes to organization, technical content, format, etc.) _____

_____

_____

BRL Report Number BRL-TR-3318 Division Symbol _____

Check here if desire to be removed from distribution list. ____

Check here for address change. ____

Current address: Organization _____
Address _____

_____

_____

DEPARTMENT OF THE ARMY
Director
U.S. Army Ballistic Research Laboratory
ATTN: SLCBR-DD-T
Aberdeen Proving Ground, MD 21005-5066

OFFICIAL BUSINESS

BUSINESS REPLY MAIL
FIRST CLASS PERMIT No 0001, APG, MD

Postage will be paid by addressee.

Director
U.S. Army Ballistic Research Laboratory
ATTN: SLCBR-DD-T
Aberdeen Proving Ground, MD 21005-5066

NO POSTAGE
NECESSARY
IF MAILED
IN THE
UNITED STATES